

The Caltech Faint Galaxy Redshift Survey XII: Clustering of Galaxies¹

David W. Hogg^{2,3}, Judith G. Cohen⁴, and Roger Blandford⁵

ABSTRACT

A clustering analysis is performed on two samples of ~ 600 faint galaxies each, in two widely separated regions of the sky, including the Hubble Deep Field. One of the survey regions is configured so that some galaxy pairs span angular separations of up to 1 deg. The median redshift is $z_{\text{med}} \approx 0.55$. Strong clustering is obvious, with every pencil-beam field containing a handful of narrow redshift-space features, corresponding to galaxy structures with sizes of 5 to 20 Mpc. The structures are not obviously organized on planes, though one prominent, colinear triplet of structures is observed, spanning ~ 20 Mpc. This may be evidence of a filament. A galaxy–galaxy correlation function calculation is performed. No significant evolution of clustering (relative to stable clustering) is found in the redshift range $0.3 < z < 1.0$. This is not surprising, since uncertainties in the correlation amplitude estimated from surveys like these are large; field-to-field variations and covariances between data points are both shown to be significant. Consistent with other studies in this redshift range, the galaxy–galaxy correlation length is found to be somewhat smaller than that predicted from local measurements and an assumption of no evolution. Galaxies with absorption-line-dominated spectra show much stronger clustering at distances of < 2 Mpc than typical field galaxies. There is some evidence for weaker clustering at intermediate redshift than at low redshift, when the results presented here are compared with surveys of the local Universe. In subsets of the data, the measured pairwise velocity dispersion of galaxies ranges from 200 to 600 km s^{-1} , depending on the properties of the dominant redshift structures in each subset.

Subject headings: galaxies: evolution — galaxies: statistics — large-scale structure of universe – methods: statistical

¹ Based on observations made at the W. M. Keck Observatory, which is operated jointly by the California Institute of Technology and the University of California; and at the Palomar Observatory, which is owned and operated by the California Institute of Technology.

² Institute for Advanced Study, Olden Lane, Princeton NJ 08540, USA; hogg@ias.edu

³ Hubble Fellow

⁴ Palomar Observatory, California Institute of Technology, Pasadena CA 91125, USA

⁵ Theoretical Astrophysics, California Institute of Technology, Pasadena CA 91125, USA

1. Introduction

Numerical simulations of the growth of large scale structure (LSS) in the Universe predict that galaxies at the present day ought to lie on sheets or filaments of thickness a few Mpc, separated by distances of tens to hundreds of Mpc, and that these structures have been forming from early times right up to the present day (eg, Buryak et al 1994; Bond et al 1996; Colberg et al 1999). As in the numerical models (although perhaps less clearly), galaxies in the local Universe are indeed observed to populate such structures (eg, J oeveer et al 1978; Geller & Huchra 1989; da Costa et al 1994; Shectman et al 1996; Vettolani et al 1997). However, the evolution of these structures with cosmic time has not been established empirically in more than a limited way.

In principle, almost any observable aspect of LSS evolution is a strong function of cosmological parameters, including the density and age of the Universe, the nature of the dark matter, and the spectrum of initial perturbations. In accordance with the general principle that all cosmological tests are much more difficult than they at first appear, the observational situation has turned out to be disappointing, since almost any apparent evolutionary behavior, especially on small scales, is explained not just as an evolution of the LSS itself but is combined with an evolving relationship between mass and light (eg, Baugh et al 1999; Pearce et al 1999), which is to a large extent unconstrained, both theoretically and observationally. Even measurements of clustering with a time baseline out to redshifts $z > 3$, which have a huge cosmological “lever arm” are thought to place stronger constraints on the bias than the growth of structure (Steidel et al 1998; Giavalisco et al 1998; Adelberger et al 1998)!

Since theoretical predictions are turning out to be soft, the Caltech Faint Galaxy Redshift Survey (CFGRS) has the goal of contributing to an empirically based history of galaxies in the Universe, which will constrain detailed theories. In what follows, we use a pair of redshift samples, containing over 1000 galaxies to redshift unity, and spanning a range of angular separations from arcseconds to degrees, to constrain the sizes, abundances, morphologies, masses, and evolution of galaxy structures as a function of cosmic time from when the Universe was roughly half its present age to the current epoch.

After the catalogs of galaxy spectra and photometry are described in Section 2, a traditional galaxy–galaxy correlation function is measured in Section 3. The pairwise velocity dispersion of galaxies is investigated in Section 4. Highly significant groups of galaxies are identified in one of our survey regions in Section 5. The sizes and morphologies of these structures are investigated in Section 6. Our conclusions are summarized in Section 7.

Unless mentioned otherwise, the adopted world model is $H = 60 \text{ km s}^{-1} \text{ Mpc}^{-1}$ (or $h = 0.6$), $\Omega_M = 0.3$, and $\Omega_\Lambda = 0.0$. All magnitudes are Vega-relative.

2. The catalogs

This study makes use of large faint galaxy redshift samples from the CFGRS, in two regions of the sky, one centered on 00 53 23 12 33 58 (J2000), known as the “J0053+1234 region” the other centered on 12 36 49 62 12 58 (J2000), known as the “HDF region”. The HDF region is centered on the Hubble Deep Field image taken with the Hubble Space Telescope (Williams et al 1996).

2.1. The J0053+1234 region

In a previous paper (Cohen et al 1999a) redshifts were presented from a survey in a 2.0×7.3 arcmin² field, J0053+1234. Redshifts were obtained for 139 galaxies and identifications were made of 24 Galactic stars in a flux-limited sample of 195 sources to 2.2 μ m flux limit $K \leq 20$ mag. The sample is 84 percent complete at $K \leq 20$ mag. The redshifts go to $z = 1.44$, with the median extragalactic redshift $z = 0.58$. This sample is, by itself, inadequate for study of galaxy clustering. The size of the field is determined primarily by the properties of the Low Resolution Imaging Spectrograph (LRIS; Oke et al 1995) at the Keck Observatory, used for all of our spectroscopic observations; the field corresponds to only $\sim 1 \times 3$ Mpc² (proper) in our cosmology at typical redshifts of roughly one half.

To study spatial baselines of 10 to 30 Mpc, it is necessary to span angular extents of 1 deg. Given limits on available observing time, it is impossible at present to obtain a complete redshift sample to this depth over a contiguous solid angle of this diameter. In the 0053+1234 region, as will be described in more detail elsewhere (Cohen et al in preparation), six additional patches of sky (“subfields”) were observed, distributed over a 1.2×1.2 deg² area on the sky, surrounding the main J0053+1234 subfield. The configuration of the subfields is shown in Figure 1. The displayed area of each subfield corresponds to the area covered by spectroscopically observed sources. Table 1 gives various properties of the subfields, including the offsets of their centers from the center of the main subfield.

For efficiency, the selection of sources (performed with LRIS images taken in the R band) was not designed to produce complete samples in all of the subfields. The R -band photometry consists of 3-arcsec diameter focal-plane aperture magnitudes. Bright sources with $R < 22$ mag were eliminated to reduce the fraction of low redshift sources and thereby reduce telescope time involved in obtaining a significant sample with $z \sim 0.5$. Faint sources with $R > 23.5$ mag were also removed, as the probability of successful spectroscopic identification in only 2 hours of integration is not high. In addition, obviously stellar sources with $R < 22.5$ mag were avoided, although a few were observed nonetheless given the vagaries of slitmask design and the need for bright setup sources with which to align the masks. Furthermore, even within the restricted magnitude range $22 \leq R \leq 23.5$ mag, not all sources were observed. However, a large enough number of slitmasks were used in each field to wash out any spatial structure in the selection function. Figure 2 shows the histogram of R -band magnitudes for all galaxies in each subfield. Although the selection

function is complicated, it is entirely based on 3-arcsec diameter R -band magnitudes; in principle all important information about the selection function is therefore contained in Figure 2.

The spectroscopic observations have a resolution corresponding to $\approx 100 \text{ km s}^{-1}$. The redshifts and galaxy spectral classes in the new subfields were determined as in the main subfield (described in Cohen et al 1999a). The numbers of galaxies with measured redshifts and other field information are given in Table 1. The redshift completeness within the sample of sources observed exceeds 90 percent in all the subfields. The total sample of galaxies in the 0053+1234 region with known redshifts is 729, with median redshift $z_{\text{med}} = 0.55$. Figure 3 shows redshift histograms for the subfields. The J0053+1234 sample is comparable in size to the entire CFRS survey (Crampton et al 1995).

2.2. The Hubble Deep Field region

The CFGRS also has obtained and compiled 610 galaxy redshifts in a sky region centered on the HDF. The sources in this region are selected in the R band. The sample is 92 percent complete to $R = 24$ mag in the deep HST-imaged portion of the HDF region and 92 percent complete to $R = 23$ mag in a circular field of 8 arcmin diameter centered on the deep portion. The imaging data, source selection procedures, and redshift catalog are described elsewhere (Hogg et al 2000; Cohen et al 2000). Figures 2 and 3 show the histograms of R -band magnitudes and redshifts for all galaxies in the HDF region.

2.3. Random catalogs

The studies of galaxy clustering presented below require comparison with a random or Monte-Carlo sample with little or no clustering but identical selection criteria, in terms of sky position, magnitude and redshift.

A representative redshift distribution was constructed for the galaxies in each one-magnitude-wide bin in R magnitude by smoothing the observed redshift distribution of galaxies in the redshift bin with a gaussian of $\sigma = 3 \times 10^4 \text{ km s}^{-1}$ in rest-frame velocity. Random catalogs were created for each region by assigning to each real galaxy position 100 new redshifts chosen from the smoothed redshift distribution constructed for galaxies in that real galaxy’s magnitude bin. This procedure results in samples with good approximations to the angular and radial selection functions of the true samples, including the complication that the source selection criteria are different in the different fields. Note that the random catalog is 100 times the size of the real catalog.

Because there is a small but significant angular clustering of faint galaxies, the random sample does not have strictly vanishing spatial correlations. However, the angular correlation length of faint galaxies to $R \approx 24$ is ≈ 0.3 arcsec (Brainerd et al 1995). Typical galaxy–galaxy separations

in the sample are on the order of a few Mpc, corresponding to hundreds of arcsec at the typical redshifts, so the bias introduced by this non-vanishing angular correlation is very small.

3. Galaxy–galaxy correlation function

The standard statistic for galaxy clustering is the galaxy–galaxy correlation function. The three-space correlation function $\xi(r)$ is not directly computed here, because there are significant redshift-space distortions. Rather, a projected correlation function $\omega(R_\perp)$ is found through the angular correlation of galaxies close in redshift. For each galaxy in the real catalog (signified by “D” for “data”), the number of other galaxies in the D catalog, within $\Delta v_r = 1000 \text{ km s}^{-1}$ in rest-frame radial velocity, is found in a set of perpendicular proper distance R_\perp bins to make the number of data-data (DD) pairs. For each galaxy in the D catalog, the number of galaxies in the random (“R”) catalog within Δv_r is found in the same set of R_\perp bins (and divided by 100) to make the DR pairs. For each galaxy in the R catalog, the number of galaxies in the R catalog within Δv_r is found (and divided by 10^4) to make the RR pairs. The correlation function estimator is

$$\omega(R_\perp) = \frac{DD - 2DR + RR}{RR} \quad (1)$$

(Landy & Szalay 1993).

Only galaxies in the redshift range $0.10 < z < 1.15$, where the CFGRS is expected to be substantially complete (Hogg et al 1998), were used in the correlation function estimation.

This correlation function estimate is to be compared with a projection of the three-space correlation function $\xi(r)$ of the form

$$\omega(R_\perp) = \int_{-\Delta v_r}^{\Delta v_r} \xi \left(\sqrt{r^2 + \frac{v_r^2}{H(z)^2}} \right) \frac{dv_r}{2\Delta v_r} \quad (2)$$

where Δv_r is the 1000 km s^{-1} velocity width used in the estimation, and $H(z)$ is the Hubble constant as a function of redshift

$$H(z) = H_0 \sqrt{\Omega_M (1+z)^3 + \Omega_k (1+z)^2 + \Omega_\Lambda} \quad (3)$$

3.1. Results

The results of the correlation function estimation in the 0053+1234 region are shown in Figures 4 and 6. Results of the estimation in the HDF region are shown in Figure 5. Error bars on the points are 1σ , computed by bootstrap resampling the D catalog. It is important to note that these bootstrap-resampling error bars do not include uncertainties due to the specific R sample used (though this makes only a tiny contribution to the overall error budget) nor uncertainties due

to sample variance, which, with a sample this small, could be quite large. Only intercomparison of similarly surveyed fields will provide an empirical estimate of the uncertainties due to sample variance. On the other hand, the bootstrap errors may be expected to overestimate the Poisson variance in measures of the correlation function like those shown in Figures 4 and 6 (Mo et al 1992). The error bars (and their covariances) are discussed at more length below.

Figures 4 and 5 show the projected correlation function $\omega(R_{\perp})$ for the two samples split into three redshift intervals. These figures show that there is no evidence for strong evolution in the proper correlation length with redshift, although the proper correlation length is smaller in the highest redshift subsample of the 0053+1234 sample, and smaller in the lowest redshift subsample of the HDF sample. The Figures also show a theoretical correlation function which is the appropriate line-of-sight projection of

$$\xi(r) = \left(\frac{r}{r_0}\right)^{-\gamma} \quad (4)$$

where the correlation length r_0 is set to 3.5 proper Mpc with $h = 0.6$ and the exponent γ is set to 1.8.

The HDF sample shows smaller correlation lengths (weaker clustering) than the 0053+1234 sample. This could be due in part to the fact that the HDF region was selected to be “empty”; i.e., devoid of large, bright galaxies, quasars, or radio sources (Williams et al 1996). Since this clustering analysis probes the non-linear regime, such selection criteria can strongly bias the results. This explanation is supported by the much lower clustering amplitude in the lowest redshift bin (Figures 5 and 7), which is the bin most affected by avoidance of bright galaxies. It has been shown in models of structure formation that underdense regions of the Universe show a lower overall clustering amplitude, although the shape (ie, exponent) of the correlation function may be more universal (eg, Scoccimarro et al 1999).

Figure 6 indicates that when the galaxies are separated by spectral type (Cohen et al 1999a), the absorption-line-dominated galaxies show stronger correlations at small separations, as is seen in the local universe (eg, Davis & Geller 1976; Hermit et al 1996; Willmer et al 1998). Of course the sample of absorption galaxies is small (only 121), so sample variance may make this result somewhat uncertain. One indication that this may be important is that the points are not well-fit by a power-law correlation function. Figure 6 also shows that there is not a very strong dependence of the clustering on absolute galaxy luminosity. For the purposes of this test, galaxy luminosities were estimated in the rest-frame R band, using the redshift and k-corrections from the literature (Poggianti 1997). A galaxy was classified as having “high luminosity” if its rest-frame R -band luminosity was estimated to be brighter than $L^*/4$ where L^* is taken from the evolving models of Poggianti (1997). The fact that the luminosity trend found in the local Universe (eg, Willmer et al 1998) was not confirmed may be a consequence of the small sample size.

Correlation function models of the form (4) with $\gamma = 1.8$ fixed were fit to the points in Figures 4 and 5 by least-squares, using the bootstrap uncertainties. The best fits and uncertainties,

computed by the one-parameter condition $\chi^2 < \chi_{\text{best}}^2 + 1$ where χ_{best}^2 is the best-fit value of χ^2 (Press et al 1992), are plotted in Figure 7. The figure also shows that the results presented here are consistent with other studies.

Figure 7 contains a line which illustrates the prediction of “stable clustering,” the best no-evolution model for small-scale clustering of galaxies in which virialized groupings of different scales separate without growing in the expanding Universe. If the small-scale clustering of galaxies is basically accounted for by the presence of groups whose proper number densities and radii do not evolve with time, then the clustering length will decrease with increasing radius as the mean cosmic density rises (because the clustering radius is defined to be the radius at which the overdensity is unity). For a correlation function of the form (4), clustered density falls with radius as $r^{-\gamma}$ and cosmic mean rises with redshift as $(1+z)^3$, so the stable clustering prediction is that the proper correlation length decreases with radius as $(1+z)^{-3/\gamma}$.

More detailed theoretical models, based on extensions of the cold dark matter hypothesis to include the relationship between observable galaxy clustering and mass clustering, make predictions which are remarkably similar to those of stable clustering (Baugh et al 1999; Pearce et al 1999). These models are also shown in Figure 7.

All the studies of galaxies at redshifts $z > 0.2$ show smaller correlation lengths than expected based on the surveys of the local Universe and the assumption of stable clustering. This evolution result should be treated with caution, because galaxies observed in the $z > 0.2$ samples have been selected and photometered with data of different qualities and spatial resolutions, observed in different photometric bandpasses, and collected in samples with very different field areas and numbers of sources. Any individual study, taken by itself, including the present study, is at least marginally consistent with stable clustering.

3.2. Error bars

It is very important to note that the results from the two sky regions studied in this work differ by significantly more than their shot-noise (as estimated by bootstrap resampling) error bars. Of course the field-to-field variations give a much more secure estimate of the true uncertainties than bootstrap resampling in individual sky regions.

One difficult point of comparison with other studies is in the size of the error bars; there is no agreement about how such error bars should be measured. In particular, some (e.g., Carlberg et al 1997) divide bootstrap error bars by $\sqrt{3}$ based on an analysis of the statistical properties of bootstrap resampling (Mo et al 1992). This correction is not made here. Some base error bars on internal field-to-field variations. One such study, the CFRS (Le Fèvre et al 1996), shows error bars significantly smaller than the field-to-field variations observed in the present work, despite having smaller numbers and similar field sizes. The field-to-field variations observed here agree with those found in the CNOC survey (Carlberg et al 2000a).

Very few surveys, if any, consider the covariances between the error bars on separate points of the angular correlation function, even though it is clear from the analysis techniques that such covariances must be strong. Fortunately, with the bootstrap technique, it is possible to measure these covariances. The covariance matrix (in the form of correlation coefficients r_{ij} defined by

$$r_{ij} \equiv \frac{\sigma_{ij}}{\sigma_i \sigma_j} \quad (5)$$

where σ_{ij} is the covariance between data points i and j and σ_i is the square root of the variance of data point i) for the first ten “whole sample” points in Figure 6 is

$$\begin{bmatrix} 1.00 & 0.28 & 0.18 & 0.26 & -0.11 & 0.03 & 0.11 & -0.13 & -0.10 & 0.07 \\ 0.28 & 1.00 & 0.14 & 0.13 & -0.30 & 0.29 & 0.03 & -0.52 & -0.22 & -0.03 \\ 0.18 & 0.14 & 1.00 & 0.12 & -0.11 & -0.04 & 0.05 & -0.06 & 0.32 & -0.25 \\ 0.26 & 0.13 & 0.12 & 1.00 & -0.09 & 0.04 & 0.22 & 0.04 & 0.00 & -0.13 \\ -0.11 & -0.30 & -0.11 & -0.09 & 1.00 & -0.01 & 0.04 & 0.11 & 0.11 & 0.35 \\ 0.03 & 0.29 & -0.04 & 0.04 & -0.01 & 1.00 & 0.30 & -0.15 & -0.12 & -0.05 \\ 0.11 & 0.03 & 0.05 & 0.22 & 0.04 & 0.30 & 1.00 & 0.46 & 0.13 & 0.15 \\ -0.13 & -0.52 & -0.06 & 0.04 & 0.11 & -0.15 & 0.46 & 1.00 & 0.23 & -0.09 \\ -0.10 & -0.22 & 0.32 & 0.00 & 0.11 & -0.12 & 0.13 & 0.23 & 1.00 & 0.07 \\ 0.07 & -0.03 & -0.25 & -0.13 & 0.35 & -0.05 & 0.15 & -0.09 & 0.07 & 1.00 \end{bmatrix} \quad (6)$$

It is clear that many of the covariances are large and ought to be taken into account in estimating error regions. Furthermore, this matrix only represents covariances from shot noise, and not the even more significant covariances expected from the fact that the correlation function grows by gravitational clustering (eg, Scoccimarro et al 1999). When χ^2 is computed using the entire covariance matrix rather than just the individual data-point variances, the preferred ranges on the correlation length r_0 actually go down (i.e., improve) by tens of percent. This statement is true for this study, but will not be true in general, because the values and signs of the covariances depend on the survey size and geometry, along with the analysis technique. In many cases, inclusion of the covariances will loosen constraints on r_0 . The fact that the covariances affect the confidence intervals, however, demonstrates that such covariances should be taken into account in future studies.

4. Pairwise velocity dispersion

The pairwise velocity dispersion (roughly the average radial velocity difference between pairs of nearby galaxies) is a combined measure of the mean mass density of the Universe and the amplitude of the power spectrum on relatively small scales (eg, Davis et al 1985). Local measurements vary somewhat by survey and technique but are generally in the range 300 to 600 km s^{-1} (Davis & Peebles, 1983; Marzke et al 1995; Somerville et al 1997b; Landy et al 1998).

In the previous Section, the correlation function of galaxies was estimated from line-of-sight projections which are insensitive to line-of-sight velocities. However, just as the transverse correlation function can be measured, so can a line-of-sight velocity correlation function, which is a convolution of the real-space two-point correlation function and the pairwise velocity distribution of galaxies. The procedure is to compute a two-dimensional correlation function, as a function

of both transverse separation and line-of-sight velocity difference, and then fit to models of the correlation function consisting of a radial power-law convolved with a line-of-sight velocity dispersion. The estimator is the same as that used to measure the transverse one-dimensional correlation function, but applied to two-dimensional maps of the numbers of pairs in the D and R catalogs. The fits to the two-dimensional correlation function provide similar correlation lengths to those derived from the fits to the one-dimensional function, although with larger uncertainties.

The best-fit velocity dispersions are found to vary strongly from field to field and from redshift interval to redshift interval, over the range $200 < \sigma_v < 600 \text{ km s}^{-1}$. The reason for this variation is that although the prominent redshift features or groups found in the pencil-beam samples contain only about half of the galaxies, they contain the vast majority of the velocity-space galaxy pairs. This means that any measurement of pairwise velocity dispersion will be dominated by the particular galaxy groups found in that region, in that redshift range. The pairwise velocity dispersion is a statistic strongly dominated by the highest density regions of a survey. This is not a new result; indeed, local measurements of this velocity dispersion in surveys of 10^3 to 10^4 galaxies are strongly affected by the inclusion or exclusion of the richest groups or clusters (eg, Marzke et al 1995, Somerville et al 1997b). This is also true of the simulations (Somerville et al 1997a). Surveys including several or many 10^4 galaxies may be large enough to give stable results (Landy et al 1998).

5. Galaxy structures

The redshift histograms for the fields are shown in Figure 3, along with the radial velocity selection functions implied by the random catalogs. As has been noted previously (eg, Broadhurst et al 1990; Crampton et al 1995; Cohen et al 1996a; Cohen et al 1996b; Koo et al 1996), these “pencil-beam” redshift samples exhibit extremely strong clustering along the line of sight in redshift space. In the main subfield in the J0053+1234 region, with its complete sample, we estimated (Cohen et al 1996a) that more than half of the galaxies lie in the five strongest redshift features, which, except for one with a very high velocity dispersion, probably correspond to poor groups of galaxies. The spatial distributions of the galaxies in these redshift features support this (Cohen et al 1996a); they are non-uniform with little central concentration (except in the strongest feature at $z = 0.58$). Similar conclusions were reached in the HDF region (Cohen et al 1996b). These redshift features are well-sampled to $z = 0.9$ and appear to persist to higher redshifts. At all redshifts, galaxies are often found in pairs, presumably merging (eg, Carlberg et al 2000b). It is apparent from Figure 3 that all the subfields show these redshift features.

Five of the redshift features may correspond to Abell richness class -1 or greater galaxy clusters, ie, clusters containing more than 20 galaxy members with absolute magnitudes brighter than two mag fainter than the absolute magnitude of the third brightest member. These include the $z = 0.58$ feature in the J0053+1234 main subfield, the $z = 0.175$ feature in the J0053+1234 19 West subfield, and three features at $z = 0.516$, 0.560 , and 0.848 in the HDF region. These

structures have velocity dispersions above 500 km s^{-1} and tens of galaxies within the brightest few magnitudes. The presence of these five rich structures in our combined samples seems reasonable; an extrapolation to $z = 0.8$ of the areal density of the sparsest clusters in the Palomar Distant Cluster Survey (Postman et al 1996) predicts that we should find some of these true clusters.

The statistics of these redshift-space features are discussed elsewhere (Cohen et al 1996a, 1996b, 2000). Briefly, they tend to have velocity dispersions of $\sim 300 \text{ km s}^{-1}$, with large uncertainties since they approach the redshift measurement uncertainties of $\sim 100 \text{ km s}^{-1}$ (in line-of-sight rest-frame velocity). The galaxies in the features are spread across the pencil-beam subfields, each of which spans a few proper Mpc at the redshifts of interest. Typical comoving line-of-sight distances between adjacent features in a single subfield is $\sim 100 \text{ Mpc}$. The distribution of comoving radial separations between the redshift-space features shows little evidence of a feature near $100 h^{-1} \text{ Mpc}$ and no evidence for periodic structures seen in previous studies (Broadhurst et al 1990).

The transverse size of the individual subfields is $8' \equiv 3 \pm 0.5$ proper Mpc over most of the redshift interval of interest. We introduce a proper longitudinal coordinate $Z \equiv ct(z)$ where $t(z)$ is the age of the universe and just deal with structures whose longitudinal extent in Z exceeds ~ 3 proper Mpc ($\equiv 250 - 350 \text{ km s}^{-1}$ over redshifts of interest). We are also interested in features whose longitudinal extent is less than the transverse separation between subfields which is roughly ~ 10 proper Mpc. Our procedure (*cf* Cohen *et al* 1998) is to examine the overdensities after rebinning the data with all widths w_Z in the range 3-10 proper Mpc and all phases and to minimize the probability of a feature arising by chance relative to a Poissonian distribution. This gives us a procedure, albeit somewhat arbitrary, for identifying and rank ordering features on the basis of their relative significance. This also allows us to include features and sub-features together. The rank-ordered (by statistical significance) features, obtained by this procedure, with the number N of galaxy members and velocity dispersions σ_v , are given in Table 2. We have chosen only the eight most significant features for the investigations of size and morphology which follow.

6. Galaxy structure size and morphology

As the seven pencils in the J0053+1234 region span nearly a degree on the sky, we can investigate the degree of clustering on larger linear scales, ~ 25 proper Mpc, than probed by the two-point correlation function. Previously (Cohen et al 1998) we have hypothesized that structures on even larger scales ($\sim 100 \text{ Mpc}$) are present in the distribution of galaxies when the universe was less than half its present age that resemble the giant voids and walls reported in the local universe (eg, J oeveer et al 1978; Geller & Huchra 1989; da Costa et al 1994; Shectman et al 1996; Vettolani et al 1997). We now have enough data to examine this hypothesis.

Much of the controversy that surrounds the description of clustering on these scales stems from inadequate, quantitative descriptions of large scale structure. When presented with data in

which at most a few large features are present, statistical measures like the two point correlation function that assume random phases, or at least a huge, fair sample of the Universe, are likely to be misleading. Furthermore, genuinely random density fields typically exhibit structures which appear, subjectively, to be non-random. Faced with these difficulties, we shall limit ourselves to a description of the structure that we have observed and a comparison with the structure that we find in control locations. (We have attempted to perform more quantitative analyses based upon the Karhunen-Loeve transformation and the “counts in cells” method but find that these do not give stable answers with these samples.)

Three of the most significant redshift features are in the vicinity of $z = 0.430$. These three features lie along the north-south axis passing through the Main subfield and they span the full degree of the J0053+1234 region. This suggests large galaxy structures that span several subfields. In order to test the hypothesis that such large structure is generic, each of the eight identified features (in Table 2) was taken in turn and the cross-correlation with individual galaxies out to large proper radii was computed. Specifically, all galaxies located within proper distances $R < 30$ Mpc of the group center were binned. These numbers were ratioed with the same for the random catalog and unity was subtracted to make a standard cross-correlation function. For comparison with a control sample, the exercise was repeated with the same group centers displaced in redshift by 0.1. The results are shown in Figure 8, with error bars on the control points found by taking the scatter among the results for each of the eight control redshift features. No individual group shows a regular, power-law cross-correlation, so it is not possible to objectively fit the individual functions. Roughly speaking, cross-correlation lengths of 5 to 20 proper Mpc are found, with large group-to-group scatter. These sizes, combined with the measured velocity dispersions of a few 100 km s^{-1} imply virial masses from a few 10^{13} to a few $10^{14} M_{\odot}$. Crossing times are several 10^9 years. The groups near $z = 0.430$ show the largest correlation lengths because there are three of them, spanning ~ 1 deg on the sky. Galaxy structures of this size have been found previously (Small et al 1999).

There is a second hypothesis that can be tested with this data set. This is that galaxies are concentrated on planes, similar to those that have been reported locally and are sometimes found in numerical simulations. In order to define a plane, we must consider three non-colinear points. For each feature (group center), any two additional galaxies outside the feature define, along with the feature center a plane. The unit normal vector (3-vector) to this plane can be constructed. The direction cosines of this normal vector are defined to be the two components of the vector transverse to the line of sight; the projection of the normal vector onto the plane of the sky. (Those galaxies which lie in the same subfield as the feature and those pairs for which the subfields are colinear with the feature, for which the planes are poorly defined, are excluded.)

The direction cosines for each triplet (two galaxies and the feature center) are plotted on a plane, for each feature and a set of controls, in Figure 9. If the features lie in prominent planes of galaxies, these will show up as clustering of points on the direction cosine plane. As usual, the controls were made by translating the features in redshift by 0.1. There is no clear evidence that

galaxies are concentrated on planes from these data.

It is notable, however, that three of the highly significant redshift features (near $z = 0.43$) are roughly colinear. Figure 10 shows the galaxy configuration in the region of these galaxy structures. They may represent part of a filament, a structure generic to the numerical simulations. Clearly studies such as these of the morphologies of large-scale structures will benefit from large, densely sampled, contiguous areas of sky. The sparse coverage of the J0053+1234 field, though necessary for probing large angular scales, is not sufficient for making definitive statements about structure morphology.

7. Summary

A clustering analysis is performed on two samples of ~ 600 faint galaxies each, in two widely separated regions of the sky. One of the survey regions is configured so that there are galaxy pairs spanning angular separations of up to 1 deg. The median redshifts of the galaxy samples are both $z_{\text{med}} \approx 0.55$.

No strong evolution of the proper galaxy–galaxy correlation length with redshift is found (relative to stable clustering), although samples of ~ 1000 sources are simply not large enough for detecting subtle changes. There is some evidence for weaker-than-stable clustering at intermediate redshift, when the results presented here are compared with surveys of the local ($z < 0.2$) Universe, but it is to be cautioned that this result depends on comparing samples selected and observed with very different techniques. Strong field-to-field variations are found, possibly emphasized by the stringent “blank-field” criteria used to select the HDF.

Galaxies with absorption-line-dominated spectra show much stronger clustering at proper distances of < 2 Mpc than typical field galaxies, in qualitative similarity to the morphological segregation observed in the local Universe.

Although pairwise velocity dispersions are measured to be in the range 200 to 600 km s^{-1} , measured value for any particular sky region and redshift interval is dominated by the prevalent individual redshift features. For this reason, no statement about the evolution in pairwise velocity dispersion is possible from these data.

Each individual pencil-beam redshift sample contains of order five significant features (“peaks”) in its redshift distribution to redshift unity. Associating the redshift features with physical galaxy structures, we have performed a three-dimensional structure–galaxy correlation analysis and find that galaxies show measurable clustering around these structures out to ~ 20 Mpc. These lengthscales are longer than the galaxy–galaxy correlation length and similar to scales of superclusters found locally and, indeed, at even higher redshifts (Lubin et al 2000). There is some evidence for filaments, although pencil-beam surveys are not ideally suited for finding them in general.

The most prominent galaxy structures have velocity dispersions of a few 100 km s^{-1} and coherence lengths of 5 to 15 proper Mpc in the adopted cosmology. These physical parameters imply masses of $\sim 3 \times 10^{13}$ to $3 \times 10^{14} M_{\odot}$. The galaxies in the structures are not obviously concentrated in walls or sheets, and no evidence is found for periodicity on very large length scales. On the other hand, this survey of spatially separated, sparsely sampled pencil beams is not extremely sensitive to all kinds of structure morphology and will be outmoded by future surveys with larger contiguous solid angle coverage.

Most importantly, large-scale structure at $z \sim 1$ does not look very different from that found locally at the present epoch.

It is a pleasure to thank Ray Carlberg, Daniel Eisenstein, Simon Lilly, Jim Peebles, Roman Scoccimarro, Todd Small and an anonymous referee for useful comments, discussions and assistance with the literature. This research is based on observations made at the W. M. Keck Observatory, which is operated jointly by the California Institute of Technology and the University of California; and at the Palomar Observatory, which is owned and operated by the California Institute of Technology. Financial support was provided under NSF grant AST 95-29170 (to RDB) and Hubble Fellowship grant HF-01093.01-97A (to DWH) from STScI, which is operated by AURA under NASA contract NAS 5-26555. This research made use of the NASA ADS Abstract Service.

REFERENCES

- Adelberger, K. L., Steidel, C. C., Giavalisco, M., Dickinson, M., Pettini, M. & Kellogg, M., 1998, *ApJ*, 505, 18
- Baugh C. M., Benson A. J., Cole S., Frenk C. S., Lacey C. G., 1999, *MNRAS*, 305, L21
- Bond, J. R., Kofman, L., Pogosyan, D., 1996, *Nature*, 380, 603
- Brainerd T. G., Smail I., Mould J., 1995, *MNRAS*, 275, 781
- Broadhurst, T. J., Ellis, R. S., Koo, D. C. & Szalay, A. S. 1990, *Nature*, 343, 726
- Buryak, O. E., Doroshkevich, A. G., Fong, R., 1994, *ApJ*, 434, 24
- Carlberg R. G., Cowie L. L., Songaila A., Hu E. M., 1997, *ApJ*, 484, 538
- Carlberg R. G., Yee H. K. C., Morris S. L., Lin H., Hall P. B., Patton D., Sawicki M., Shepherd C. W., 2000a, *ApJ*, submitted
- Carlberg R. G. et al, 2000b, *ApJ*, submitted
- Cohen J. G., Hogg D. W., Pahre M. A., Blandford R., 1996a, *ApJ*, 462, L9
- Cohen J. G., Cowie L. L., Hogg D. W., Songaila A., Blandford R., Hu E. M., Shopbell P., 1996b, *ApJ*, 471, L5

- Cohen J. G., Hogg D. W., Pahre M. A., Blandford R. D., Shopbell P. L., Richberg K., 1999a, ApJS, 120, 171
- Cohen J. G., Blandford R. D., Hogg D. W., Pahre M. A., Shopbell P. L., 1999b, ApJ, 512, 30
- Cohen J. G., Hogg D. W., Blandford R., Cowie L. L., Hu E., Songaila A., Shopbell P., Richberg K., 2000, ApJ, in press
- Colberg, J. M., White, S. D. M., Jenkins, A., Pearce, F. R., 1999, MNRAS, 308, 593
- Crampton D., Le Fevre O., Lilly S. J., Hammer F., 1995, ApJ, 455, 96
- da Costa, L. N. et al. 1994, ApJ, 424, L1
- Davis M., Geller M. J., 1976, ApJ, 208, 13
- Davis M., Peebles P. J. E., 1983, ApJ, 267, 465
- Davis M., Efstathiou G., Frenk C. S., White S. D. M., 1985, ApJ, 292, 371
- Geller M. J., Huchra J. P., 1989, Science, 246, 897
- Giavalisco M., Steidel C. C., Adelberger K. L., Dickinson M. E., Pettini M., Kellogg M., 1998, ApJ, 503, 543
- Guzzo L. et al, 2000, *Å*, 355, 1
- Hermit S., Santiago B. X., Lahav O., Strauss M. A., Davis M., Dressler A., Huchra J. P., 1996, MNRAS, 283, 709
- Hogg D. W., Cohen J. G., Blandford R., Pahre M. A., 1998, ApJ, 504, 622
- Hogg D. W., Pahre M. A., Adelberger K. L., Blandford R., Cohen J. G., Gautier T. N., Jarrett T., Neugebauer G., Steidel C. C., 2000, ApJS, in press
- Hudon J. D., Lilly S. J., 1996, ApJ, 469, 519
- Jõeveer M., Einasto J., Tago E., 1978, MNRAS, 185, 357
- Koo, D. C. et al., 1996, ApJ, 469, 535
- Landy S. D., Szalay A. S., 1993, ApJ, 412, 64
- Landy S. D., Szalay A. S., Broadhurst T. J., 1998, ApJ, 494, L133
- Le Fèvre O., Hudon D., Lilly S. J., Crampton D., Hammer F., Tresse L., 1996, ApJ, 461, 534
- Loveday J., Maddox S. J., Efstathiou G., Peterson B. A., 1995, ApJ, 442, 457
- Lubin L. M., Brunner R., Metzger M. R., Postman M., Oke J. B., 2000, ApJ in press
- Marzke R. O., Geller M. J., da Costa L. N., Huchra J. P., 1995, AJ, 110, 477
- Mo H. J., Jing Y. P., Borner G., 1992, ApJ, 392, 452
- Oke J. B. et al, 1995, PASP, 107, 375
- Pearce F. R. et al, 1999, ApJ, 521, L99
- Peebles P. J. E., 1993, *Principles of Physical Cosmology*, Princeton University Press, Princeton

- Poggianti, B. M. 1997, A&AS, 122, 399
- Postman M., Lubin L. M., Gunn J. E., Oke J. B., Hoessel J. G., Schneider D. P., Christensen, J. A., 1996, AJ, 111, 615
- Postman M., Lauer T. R., Szapudi I., Oegerle W., 1998, ApJ, 506, 33
- Press W. H., Teukolsky S. A., Vetterling W. T., Flannery B. P., 1992, *Numerical Recipes in C*, 2ed, Cambridge University Press, Cambridge
- Shectman, S. A., Landy, S. D., Oemler, A. , Tucker, D. L., Lin, H. , Kirshner, R. P., Schechter, P. L. 1996, ApJ, 470, 172
- Scoccimarro R., Zaldarriaga M., Hui L., 1999, ApJ, in press
- Shepherd C. W., Carlberg R. G., Yee H. K. C., Ellingson E., 1997, ApJ, 479, 82
- Small T. A., Ma C.-P., Sargent W. L. W., Hamilton D., 1999, ApJ, 524, 31
- Somerville R. S., Primack J., Nolthenius R., 1997a, ApJ, 479, 606
- Somerville R. S., Davis M., Primack J. R., 1997b, ApJ, 479, 616
- Steidel, C. C., Adelberger, K. L., Dickinson, M., Giavalisco, M., Pettini, M., Kellogg, M., 1998, ApJ, 492, 428
- Tucker D. L., Oemler A. Jr., Kirshner R. P., Lin H., Shectman S. A., Landy S. D., Schechter P. L., Müller V., Gottlöber S., Einasto J., 1997, MNRAS, 285, L5
- Vettolani, G. et al., 1997, A&A, 325, 954
- Willmer C. N. A., da Costa L. N., Pellegrini P. S., 1998, AJ, 115, 869

Table 1. Subfields in the J0053+1234 region

subfield	$\Delta\alpha$ (arcmin)	$\Delta\delta$ (arcmin)	Ω^a (arcmin ²)	flux range (mag)	N_z^b	f_z^c
main	0.0	0.0	15	$K < 20.0$	139	0.84
8 South	+4.6	−9.4	14	$22.0 < R < 23.5$	96	0.93
11 West	−11.7	−7.9	14	$22.0 < R < 23.5$	78	0.76
19 West	−19.3	−3.2	14	$22.0 < R < 23.5$	62	0.60
30 North	−0.6	+30.5	48	$22.0 < R < 23.5$	119	0.34
30 South	−0.3	−32.7	47	$22.0 < R < 23.5$	116	0.33
30 East	+29.5	−0.1	48	$22.0 < R < 23.5$	119	0.34
total					729	

^a Ω is the solid angle of each field.

^b N_z is the number of spectroscopically confirmed galaxies with redshifts. Spectroscopically confirmed stars have been excluded.

^c f_z is the approximate fraction of galaxies in the magnitude range whose redshifts have been measured.

Table 2. Highly significant redshift features in the J0053+1234 region

redshift	σ_v^a (km s ⁻¹)	subfield	N
0.173 ^b	473	19 West	20
0.577 ^c	404	Main	24
0.621	278	8 South	10
0.428	346	Main	10
0.676	298	Main	9
0.550	274	11 West	8
0.427	255	30 South	7
0.431	165	30 North	7

^aNo correction to the velocity dispersion σ_v was made for measurement uncertainties.

^bCombination of 3 significant sub-features.

^cCombination of 2 significant sub-features.

Caltech Faint Galaxy Redshift Survey - 0 Hour Fields

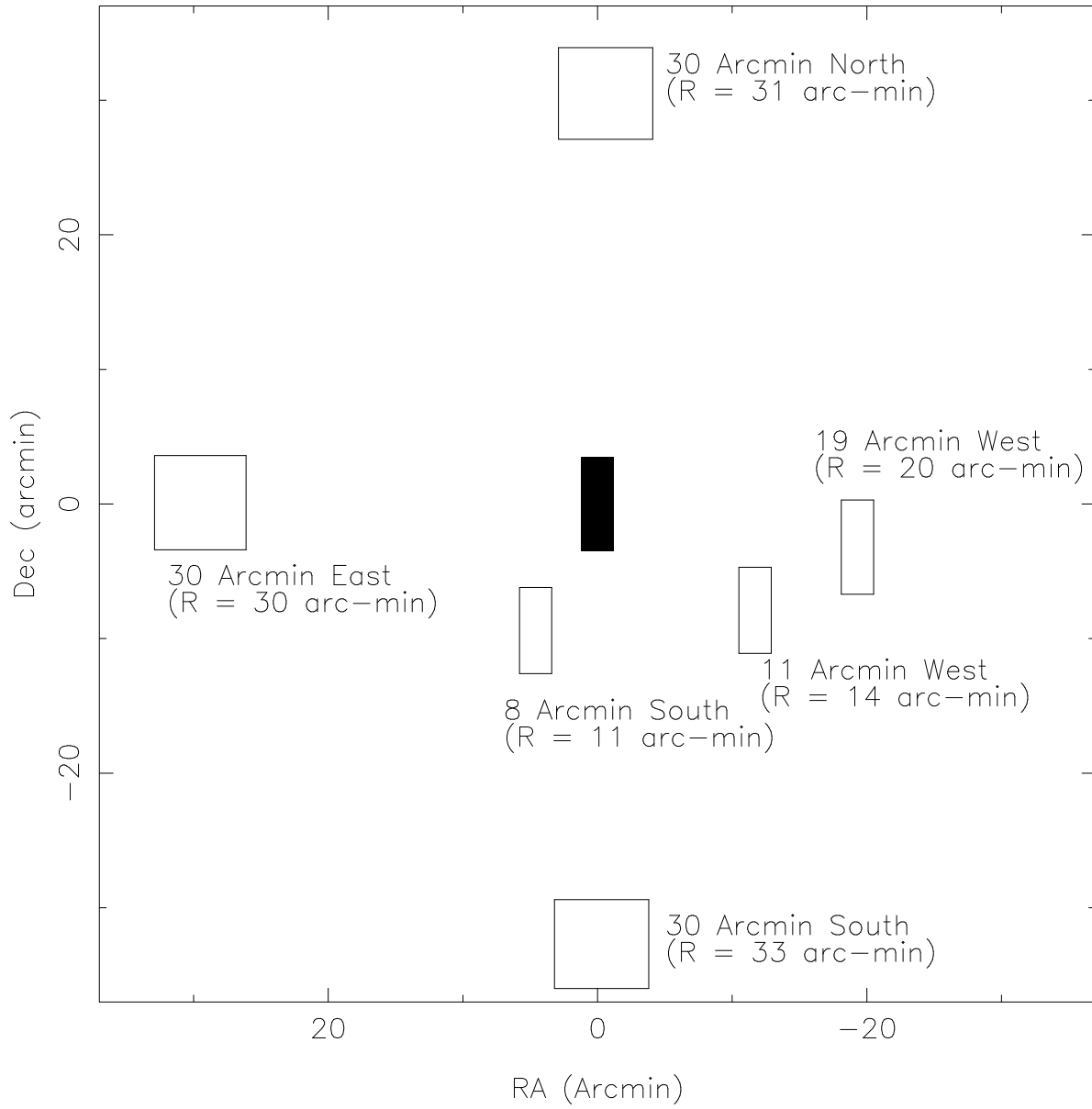
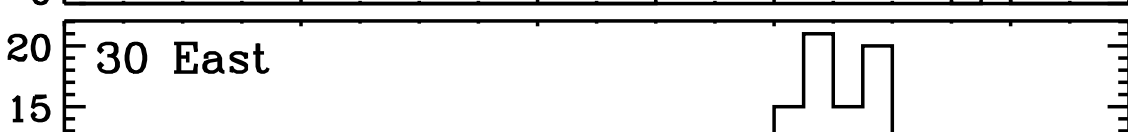
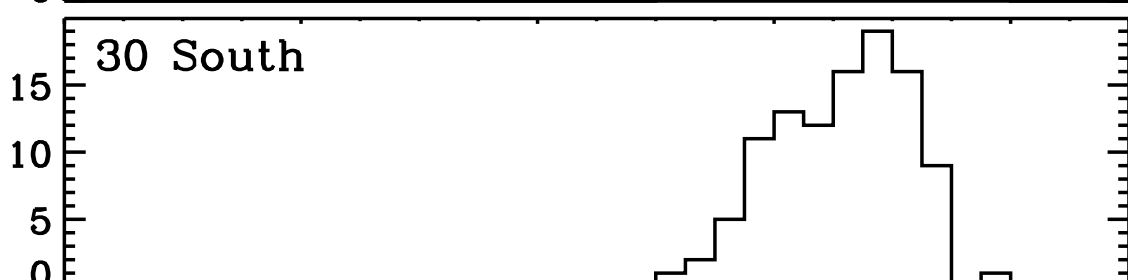
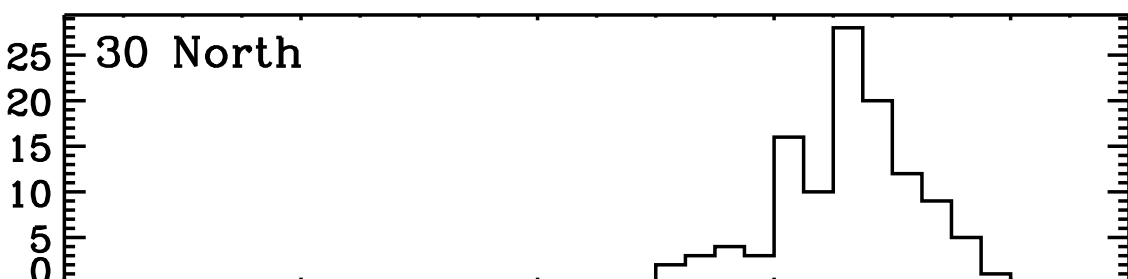
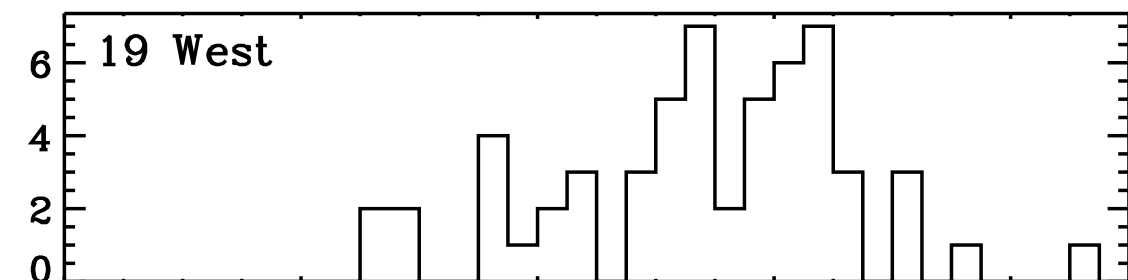
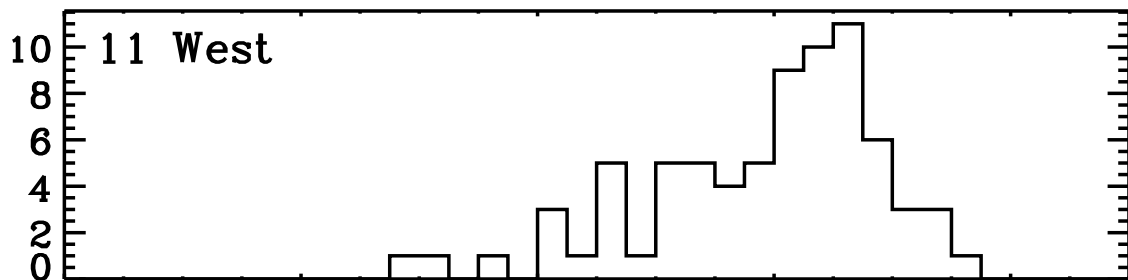
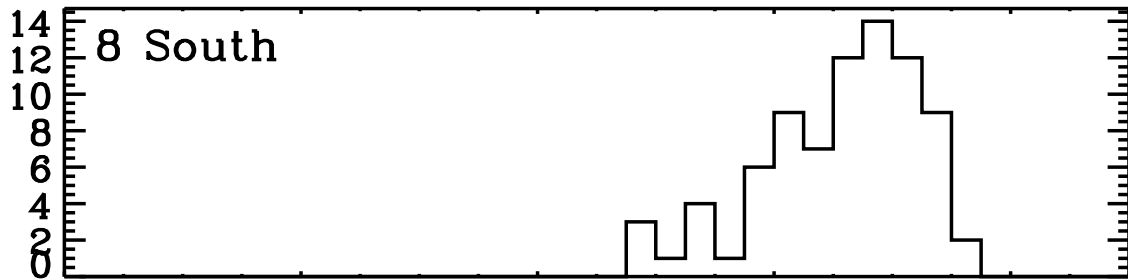
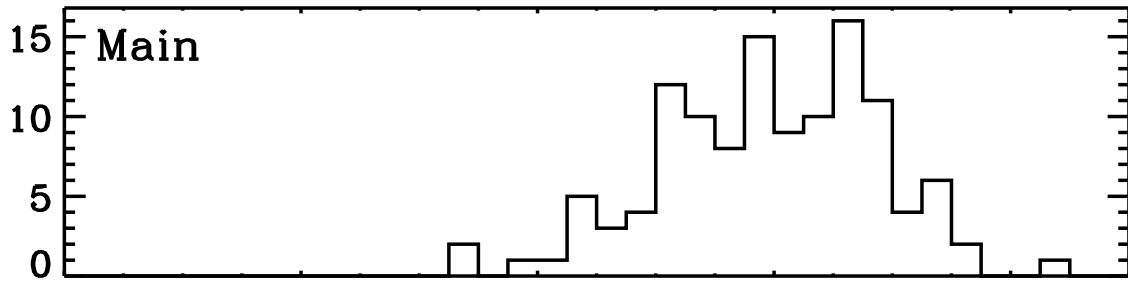


Fig. 1.— The layout of subfields in the 0053+1243 region.



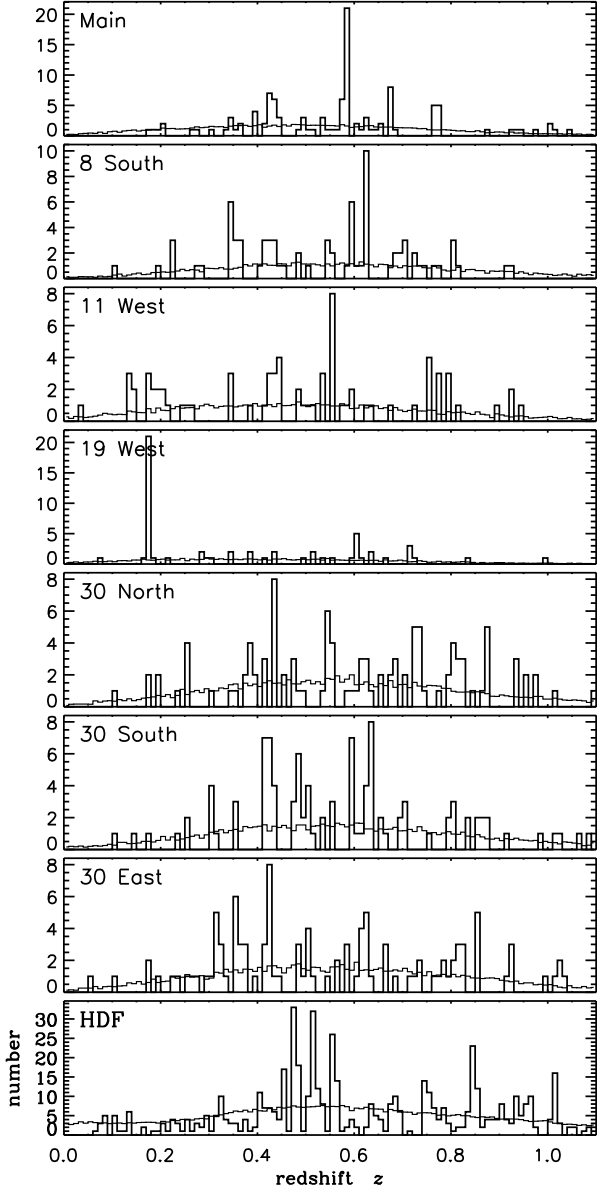


Fig. 3.— The dark histograms show the numbers of sources as a function of redshift in the subfields of the J0053+1234 region and in the HDF region. The light histogram shows the numbers in the random catalog described in the text. Because the R catalog is 100 times larger than the data catalog, the R numbers have been divided by 100. Note that different panels have different vertical scales.

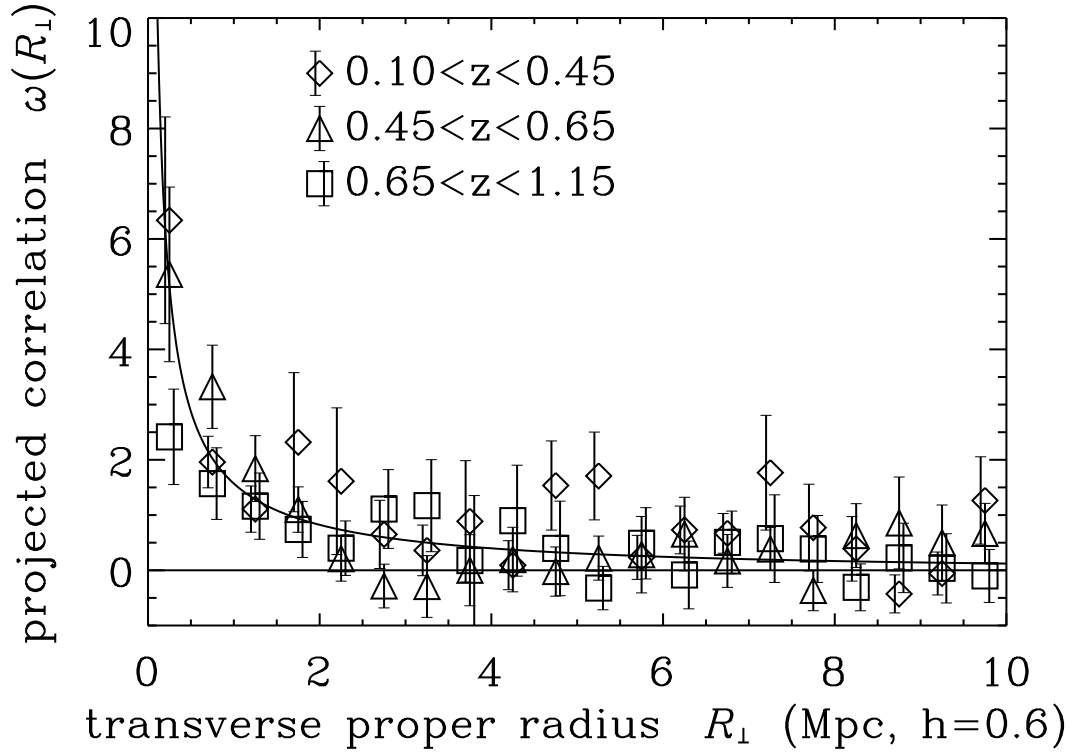


Fig. 4.— The projected correlation function in proper coordinates in the J0053+1234 region in three redshift bins. The correlation function is estimated as described in the text. The solid curve shows a correlation function of the form (4) with $r_0 = 3.5$ Mpc and $\gamma = 1.8$, projected through $\Delta v_r = 1000 \text{ km s}^{-1}$ at $z = 0.55$ according to (2).

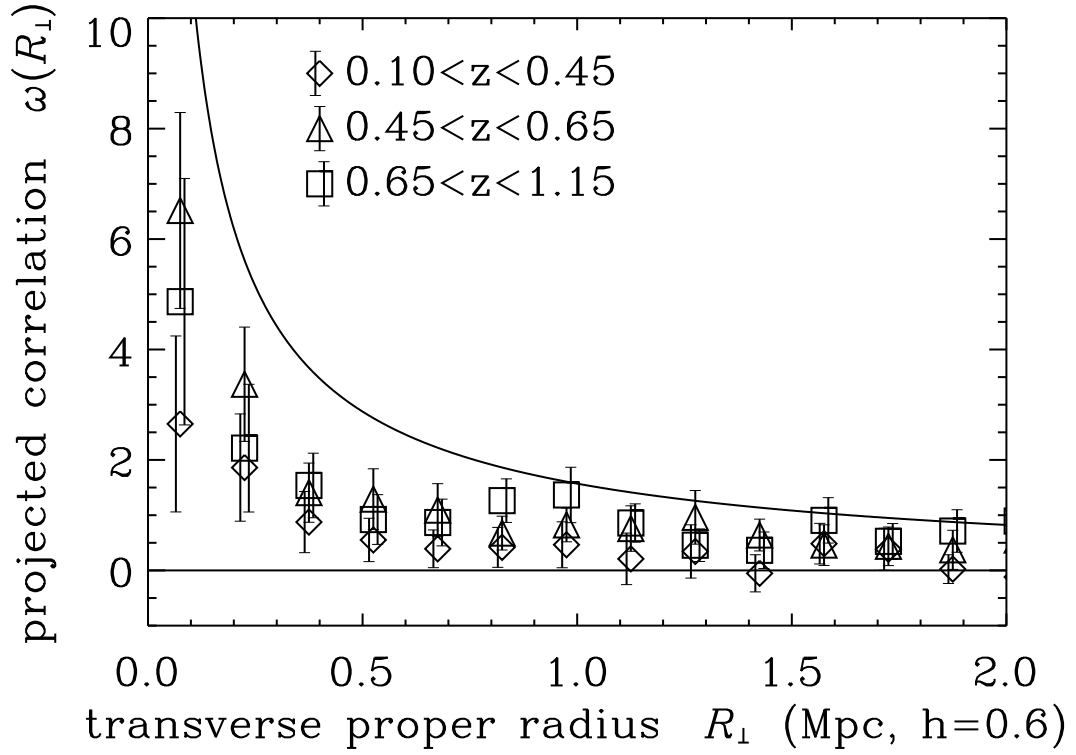


Fig. 5.— The projected correlation function in proper coordinates in the HDF region in three redshift bins. The correlation function is estimated as described in the text. The solid curve shows the same correlation function as that shown in Figure 4. Note that the horizontal axis scale is different from that in Figure 4 because the angular separation coverage is smaller in the HDF sample than in the 0053+1234 sample.

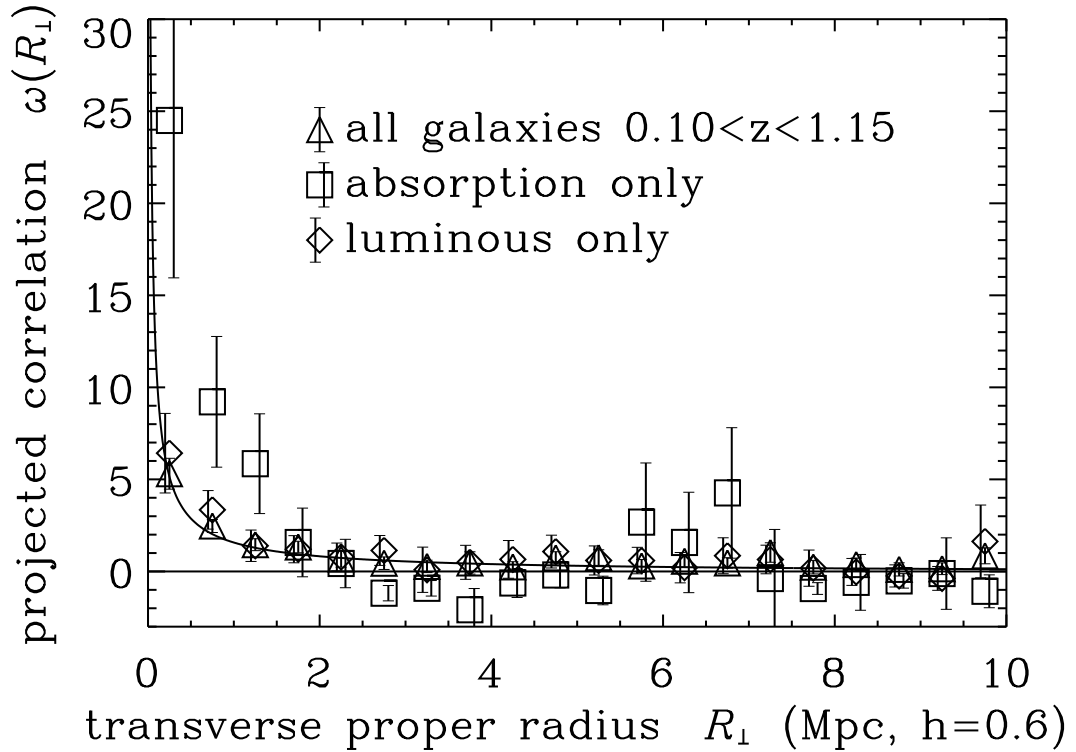


Fig. 6.— The projected correlation function in proper coordinates for the whole J0053+1234 sample, just those J0053+1234 galaxies with absorption-line-dominated spectra, and just those J0053+1234 galaxies with intrinsic luminosities (as estimated according to the text) $\log L/L^* > -0.6$. The solid curve shows a correlation function of the form (4) with $r_0 = 3.5$ Mpc and $\gamma = 1.8$, projected through $\Delta v_r = 1000 \text{ km s}^{-1}$ at $z = 0.55$ according to (2).

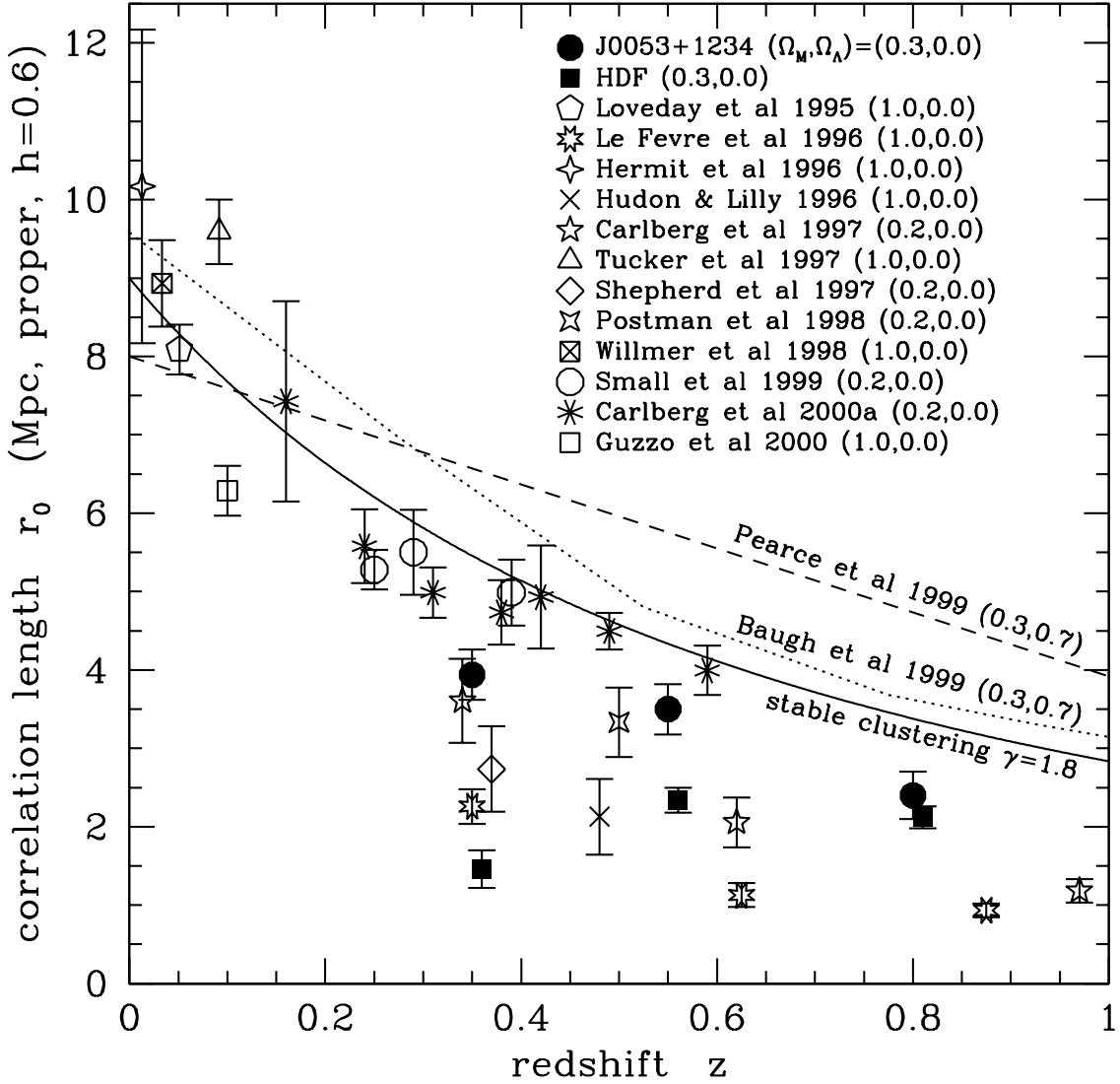


Fig. 7.— The best-fit correlation lengths r_0 in this work and from other studies. For this work (solid points), the fits were performed with γ fixed at 1.8. The solid line shows the “stable clustering” prediction (eg, Peebles 1993) for $\gamma = 1.8$ with $r_0 = 9.0$ Mpc at $z = 0$. The results of the other work have been transformed to $h = 0.6$ and proper coordinates. Error bars on the solid points are based only on bootstrap resampling and therefore represent lower limits to the true uncertainties. The error bars on the Le Fevre et al (1996) points are likely incorrect; see text. It should be noted that the other work is heterogeneous, with galaxies selected in many different ways, in different magnitude and redshift ranges, with different assumed or fit values of γ , and in different cosmographic models. See the original references for details. The dotted and dashed lines show theoretical predictions.

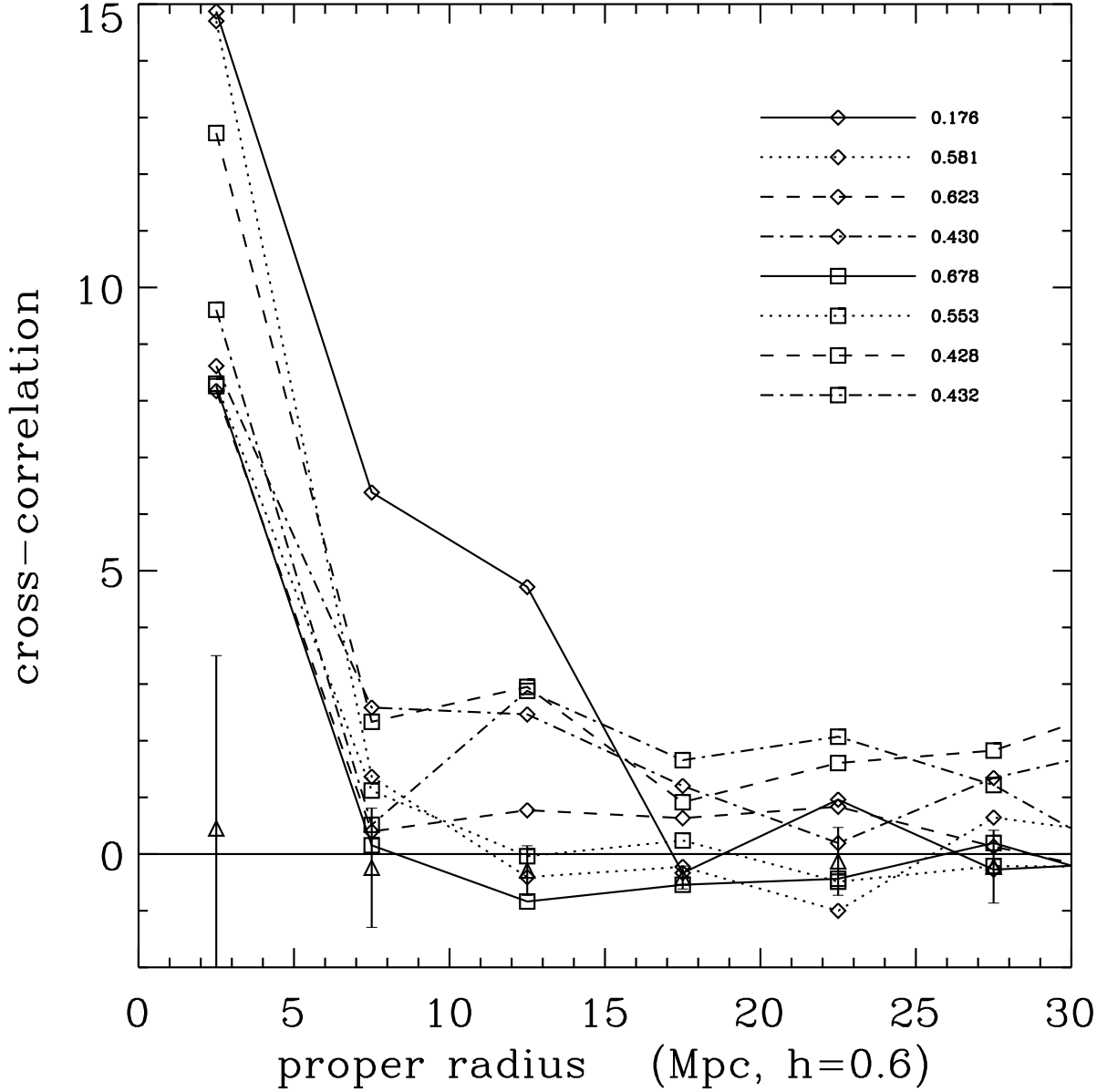


Fig. 8.— The eight group-galaxy cross-correlation functions for the eight redshift features in Table 2 and the averaged cross-correlation functions for the shifted control features (triangles). The error bars represent the control feature-to-feature scatter. Details in the text.

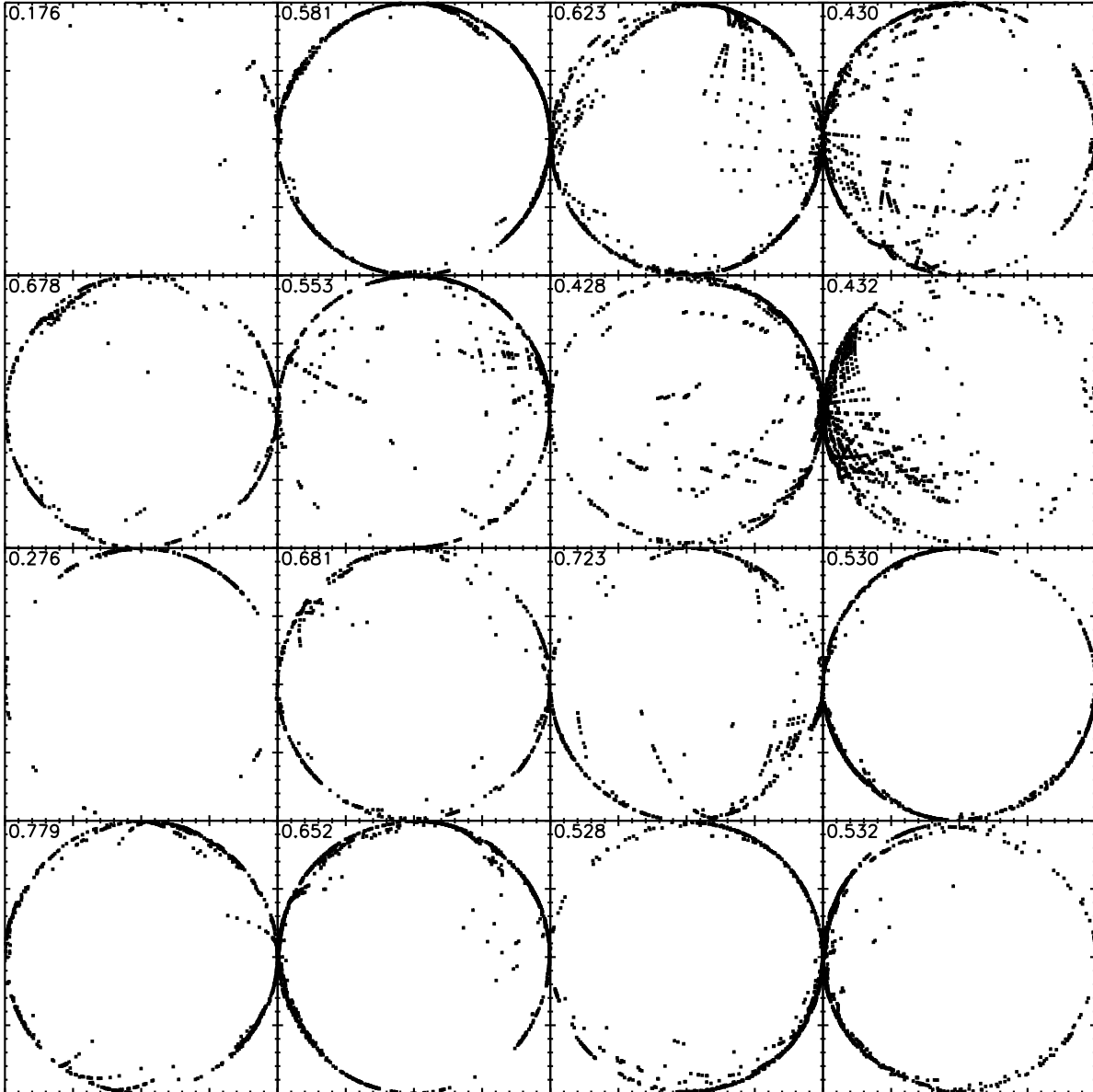


Fig. 9.— The direction cosines for pairs of galaxies relative to each of the eight groups in Table 2 (top eight panels) and for the same group centers but shifted in redshift by 0.1 (bottom eight panels). Each point in each panel shows the north–south (vertical) and east–west (horizontal) components of the unit 3-vector normal to the plane defined by each triplet composed of each pair of galaxies and the group center. Details in the text.

Fig. 10.— [NOTE TO astro-ph USER: These figures are in the archive as rdb043.gif and rdb053.gif] *(Top)* Location of galaxies in a $30 \times 30 \times 100$ proper Mpc (equivalent to cosmic time along the line of sight) region of the J0053+1234 field chosen to include three distinct redshift features near $z = 0.43$ in Table 2. The faint “ribs” connecting individual galaxies to the central “spine” (chosen to lie at the center of the main field) are perpendicular to the spine. Our typical velocity error of $200 \text{ km s}^{-1} \text{ Mpc}^{-1}$ corresponds to a distance of 2.4 Mpc along the line of sight and departures from Hubble expansion are less than ~ 7 Mpc. The radius of a galaxy symbol corresponds to $M_R^* - M_R$. The galaxies are color-coded with red corresponding to absorption line galaxies, green composite and blue emission line galaxies. Note that absorption line galaxies are more luminous and concentrated in the redshift features. It is apparent that galaxies are clustered around this concentration with correlation lengths of $\sim 20 - 30$ proper Mpc. The three principal features are roughly colinear, but, in general, there is little indication that galaxies are arranged either on planes or lines. *(Bottom)* A more typical region, with similar dimensions, displaced from that shown in the first panel by $\Delta z = 0.1$.

This figure "rdb043.gif" is available in "gif" format from:

<http://arxiv.org/ps/astro-ph/0006284v2>

This figure "rdb053.gif" is available in "gif" format from:

<http://arxiv.org/ps/astro-ph/0006284v2>